Full Paper

Plasma deposition of superhydrophobic Ag@TiO$_2$ core@shell nanorods on processable substrates[a]

Manuel Macias-Montero, Ana Borras,[*] Pablo Romero-Gomez, Jose Cotrino, Fabian Frutos and Agustin R. Gonzalez-Elipe

―――――――

M. Macias, Dr. Borras, Dr. Romero-Gomez, Prof. Cotrino, Prof. Gonzalez-Elipe
Nanotechnology on Surfaces Laboratory, Materials Science Institute of Seville (ICMS),
CSIC-University of Seville, C/ Americo Vespucio 49, Seville, E-41092, Spain
E-mail: anaisabel.borras@icmse.csic.es
Dr. F. Frutos
Applied Physic Department, E.T.S. Ingenieria Informatica (University of Seville), Avd. Reina Mercedes s/n, Seville, E-41012, Spain

―――――――

This work reports the low temperature plasma formation of Ag@TiO$_2$ nanorods consisting of a silver core and an external shell of TiO$_2$ deposited on silver coated processable substrates. Layers of supported nanorods have been analyzed by scanning electron microscopy (SEM), transmission electron microscopy (TEM) and time of flight secondary ion mass spectroscopy (TOF-SIMS). The analysis of the nanorods morphologies as a function of the preparation conditions has revealed that the effect of the plasma sheath, the high mobility of the silver and the incoming direction of the precursor moieties are key factors determining the morphology, dimensions and tilting orientation of the core@shell nanostructures. Post-annealing of the as-prepared samples at 673 K induced the crystallization of the amorphous TiO$_2$ shell into the anatase phase. The as-grown amorphous and anatase Ag@TiO$_2$ NRs surfaces present a superhydrophobic behavior with water contact angles higher than 150º, that turn into superhydrophilic through a two-step kinetic by irradiation with UV light. This wetting behavior is discussed within the framework of the Wenzel and Cassie-Baxter models,

―――――――――――――

including the effect of the water penetration in the inter-NR space during the light-mediated superhydrophobic-superhydrophilic transformation.

Introduction

During the last decade, the fabrication and processing of one dimensional (1D) supported TiO$_2$ nanostructures have deserved an ever-increasing interest because of their high performance as photocatalysts, electrodes in photovoltaic cells, nanosensors, biomaterials, self-cleaning surfaces or microfluidic components.[1] In relation with these two latter applications, the singular properties of the 1D TiO$_2$ nanostructures have prompted their use as model systems to investigate basic wetting phenomena. Among these features we can quote i) a high thermal and chemical stability, ii) a hydrophobic-superhydrophilic conversion by illumination with UV light or iii) the superhydrophobic character of high density 1D nanostructured-layers. In this context, a key feature for many applications is to succeed in reversibly controlling the wettability of surfaces (i.e., the change from hydrophobic to hydrophilic and back). This has been attempted by the application of electric fields,[2-5] heating[6-7] and light irradiation.[8] The reversible light induced superhydrophobic-superhydrophylic transition of Ag@TiO$_2$ core@shell nanofibers (NFs) is a clear example of the possibilities offered by these structures to light tuning the water contact angle (WCA) of a nanostructured surface.[9]

Typically, TiO$_2$ nanostructures comprising nanorods, nanofibers and nanotubes have been prepared by means of chemical or electrochemical routes including template methods.[10-17] High temperature annealing of Ti foils has been also intended for the preparation of this type of systems.[18] These methods involve successive drying, heating, or high temperature annealing steps that hamper their application when mild conditions are required or when the synthesis has to be carried out in a single experimental set-up. Plasma methods provide a way to circumvent part of these shortcomings[19-20] as clearly exemplified by the fabrication of

carbon nanotubes (CNTs) at temperatures much lower than with thermal CVD or hydrothermal processes.[21-23] Nano- and meso-porous TiO_2 films have been previously deposited at low substrate temperatures by plasma-enhanced chemical vapour deposition (PECVD).[24-25] The aforementioned $Ag@TiO_2$ core@shell NFs were also prepared by this technique at T > 403 K by depositing TiO_2 on a plasma oxidized silver foil.[9,26-28] A special feature of those supported $Ag@TiO_2$ core@shell NFs was that the inner silver core was formed by a 20 nm thick single crystalline thread of this metal.

In the present work we have succeeded in extending the methodology of fabrication of $Ag@TiO_2$ nanostructures from bulk silver to processable substrates, the first step required for their integration in actual devices such as solar cells or microfluidics circuits. This goal has been attempted by plasma deposition of TiO_2 on a thin silver layer deposited on flat substrates by DC sputtering. Recently, an equivalent route has been fruitfully applied for the preparation of Ag-NPs@ZnO nanorods (NRs)[29,30] characterized by a polycrystalline hollow shell of ZnO decorated in its interior with Ag nanoparticles. Herein, to tailor the shape, density and other morphological characteristics of the $Ag@TiO_2$ 1D nanostructures, we have systematically varied experimental parameters such as the deposition geometry or the temperature during the plasma deposition of TiO_2.

In the quest for manageable wetting surfaces, we have also studied the surface wetting behavior of the nanorods-arrays either as prepared or after UV irradiation to induce a hydrophobic to hydrophilic transformation. The results obtained, rationalized by applying the Wenzel and Cassie-Baxter models,[25b,31] design a complex pattern where the surface nanostructure, the intrinsic photo-activity of TiO_2 and the dependence of this latter property on its crystalline structure play critical roles.

Experimental Section

Ag@TiO$_2$ Nanorods fabrication

Fused silica slides and Si(100) wafers were covered by silver via DC sputtering from a metal wire under a pressure of 1.5 Torr of Argon and an applied voltage of 400 V. Calibration of the deposition rate allowed us to control the amount of deposited silver and to determine the equivalent layer thickness (i.e., the thickness in case that silver would have formed a continuous and compact film). The sample holder with the silver covered substrates was heated by irradiation with quartz lamps up to a maximum temperature of 430 K. The reactor consisted of a stainless-steel chamber supplied with a microwave (MW) plasma source (SLAN from Plasma Consult, Germany) in a remote configuration and directly supplied with the plasma gas, in our case oxygen at a flow rate of 21.6 sccm. A detailed description of this reactor and its working conditions can be found elsewhere.[32] Herein, in order to account for the orientation of the deposited structures, it is important to specifically describe the inner reactor geometry and other working details. **Figure 1** shows the reactor schematics highlighting the following features: i) a plasma source which is directly fed with the oxygen plasma gas, ii) a precursor dispenser placed above the substrate and iii) a pumping system, which placed below the substrate position, defines a preferential top-bottom flux of both the plasma gas and precursor fragments.

The silver covered substrates were oxidized by exposure to oxygen plasma at a temperature of 407 K during 30 minutes. As it will be discussed later, such a treatment increases the roughness of the silver substrate and promotes the mobility of the silver clusters. Similar conditions of oxygen plasma have been previously applied to the fabrication of supported hybrid nanowires.[33] For the plasma enhanced chemical vapor deposition (PECVD) of TiO_2, the reactor was supplied with oxygen and excited with a microwave power of 400 W. The Ti[OCH(CH3)2]4 precursor (Sigma-Aldrich) was dosed by passing and additional oxygen flow (0.5 – 2.5 sccm) through a stainless-steel recipient containing the precursor at 313 K. Total working pressure during deposition was 5×10^{-3} Torr. Both the line connecting this container with the chamber and the precursor shower-like dispenser were heated at $T > 353$ K

to avoid condensation of the metal-organic precursor. The oxygen flow through the precursor reservoir was used as an indirect way of controlling the amount of precursor dosed in each experiment.

Conversion of the amorphous TiO_2 shell into the anatase phase is achieved by the annealing of samples in air at 673 K for 4h.[34]

Characterization

Scanning electron microscopy (SEM) analysis of the specimen was carried out with a Hitachi S5200 field-emission microscope. The samples were examined without any specific manipulation. For transmission electron microscopy (TEM, Phillips CM200) analysis of the individual nanorods, they were scraped from the surface with a diamond tip and subsequently collected with a Holley-Carbon grid.

Time-of-Flight Secondary Ion Mass Spectroscopy (TOF-SIMS) depth profiling analysis was performed on a TOF-SIMS type ION-TOF IV instrument (IONTOF GmbH, Münster, Germany), equipped with a Bi polyatomic primary ion source, a Cs/electron impact dual source column, and a low-energy electron flood gun (for charge compensation of insulating samples).

Gracing incidence X-ray diffraction (GAXRD) studies were performed in an X`Pert Pro from Panalytical for X-Ray angles < 1º.

Water Contact angles (WCA) were determined on aged samples (i.e., stored for 30 days in a desiccator after their preparation) by the Young method with a Data Physic Instruments using small droplets of mili-Q water. The samples were irradiated with a Xe lamp (photon intensity at the position of the samples ca. 2 W cm^{-2}) and the WCA were measured after irradiation for given periods of time. Except for the original samples before irradiation where advancing and receding angles could be determined (the reported values correspond to the mean value of five measurements in different zones of the sample), only static contact angles from just one small water droplet of 5µl size were taken for the data as a function of the irradiation time. The

reason for that is that illuminated surfaces of TiO$_2$ are not static and their wetting characteristics evolve with time and exposure to visible light. This precludes the reliability of any long essay and makes that the reported values must be taken as indicative of tendencies rather than as statistically exact.

Results and Discussion

Synthesis and characterization of Ag@TiO$_2$ nanorods

Ag@TiO$_2$ nanorods (NRs) were grown on the selected processable substrates by following a three-step methodology: 1) silver deposition by DC sputtering on Si or quartz, 2) plasma oxidation of the deposited silver to get structured and chemically modified silver surfaces and 3) PECVD deposition of TiO$_2$ at 407 K. An example of the as-prepared substrates and of the effect of plasma oxidation is shown in **Figure 2**, together with the images of the final NRs obtained by TiO$_2$ deposition for 60 minutes on a silver layer of 50 nm nominal thickness and with an oxygen flow through the precursor dispenser of 0.5 sccm. The as-prepared silver layers (Figure 2a and d), consisted of a continuous and smooth film of agglomerated silver particles. In good agreement with previous studies,[27-28] after plasma oxidation the treated silver was no longer smooth neither continuous as shown in Figures 2 b) and e), where it is apparent that the oxidized substrates become highly rough and presented bare silicon areas not covered by silver. On these substrates plasma deposition of TiO$_2$ rendered a large number of core@shell NRs with a length of 550 nm and a thickness comprised between 80 nm and 250 nm depending on the deposition time (c.f., Figures 2 c) and f)). It is worthy of note that despite the inhomogeneous silver distribution in the plasma pre-treated substrate the obtained NRs were quite homogeneous, both in length and thickness. This result suggests that silver undergoes additional morphological modifications during the PECVD of TiO$_2$. We will be back to this discussion in the next section regarding the formation of tilted nanorods. TEM and time of flight secondary ion mass spectroscopy (ToF-SIMS) analysis were carried out to, respectively, characterize the internal microstructure and

compositional depth distribution of silver through the nanorod layer (**Figure 3**). The bright field TEM micrograph of a single $Ag@TiO_2$ NR in Figure 3 a) shows a high contrast between an inner core attributed to silver (30nm thick) and an external shell of titanium dioxide. Contrary to the single crystalline character of the silver threads formed in the $Ag@TiO_2$ NFs developed on bulk silver substrates,[26-27] for the $Ag@TiO_2$ NRs on processable supports the silver appears in the form of agglomerated particles mostly distributed in the core of the 1D heterostructure although isolated silver clusters can be also observed in the surface of the TiO_2 shell (Figure 3 a). This latter fact further supports the key role of the mobility of the silver clusters upon plasma and temperature activation. On other hand, complementary ToF-SIMS analysis (Figure 3 b) shows that both silver and titanium dioxide are distributed homogeneously from the top of the NRs up to their base. The appearance of silicon in the depth distribution profile before that silver and titanium signals go to zero is inherent to the open microstructure of the samples and indicates that in this NR microstructure the sputtering ions enter up to the silicon substrate before the complete removal of TiO_2 and silver.

Control of morphology and formation of tilted NRs

Different NR morphologies could be obtained by varying some process parameters, particularly the precursor dose, the thickness of the silver layer and the deposition time. In the curse of this investigation it could be determined that a minimum equivalent thickness of 20 nm of silver was required for the formation of NRs. A selection of typical microstructures is shown in **Figure 4** reporting first the effect of changing the flow of oxygen bubbled through the precursor to control its dosage. According to Figure 4 a), TiO_2 deposition for 60 minutes with an oxygen flow of 0.5 sccm renders NRs of about 550 nm long and 100 nm thick. Deposition for the same time and an oxygen flow of 1.0 sccm yields NRs with a similar thickness and a mean length of 900 nm (Figure 4 b), a result indicating that it is possible to get high aspect ratio NRs by just increasing the amount of precursor dosed in the chamber. In a limit case, when the oxygen flow was augmented to 2.5 sccm (Figure 4 c), inhomogeneous

and irregular nanostructures possessing an even higher aspect ratio (i.e., lengths in the order of 1400 nm and approximate thickness of 100 nm) were obtained. These new forms might be useful for applications requiring large specific areas.

Meanwhile, experiments carried out for 120 minutes (c.f., Figure 4 d) keeping constant the oxygen flow through the precursor at 0.5 sccm, lead to the formation of thick (100-250nm) and relatively low aspect ratio NRs. This result indicates that, once the NRs reach a critical height, they start to grow radially with an inverted-conical morphology characteristic of the self-shadowing effect presented on plasma made 1D core@shell systems,[35,36] more pronounced in the thicker nanorods (Figure 4 d). A close inspection of the SEM micrographs in Figure 4 also reveals that the long and thick NRs coexist with other shorter and thinner nanostructures. This heterogeneous distribution of NRs lengths might be related to both, deposition of TiO_2 on small size metal seeds and the shadowing effects produced by the bigger NRs. Such a hint of the existence of shadowing effects during the growth process of the NRs prompted us to prepare tilted nanostructures by playing with the directionality of the TTIP precursor flow with respect to the normal direction to the substrate. Effectively, we found that a wide range of NRs tilting angles could be obtained by varying both the angle and separation of the substrate with respect to the precursor dispenser. Details of the procedure can be also found in reference 30 where the fabrication of tilted ZnO NRs by PECVD was reported. For TiO_2, an example of the effect of the gas flow directionality is presented in Figure 4 e) where we show the cross section SEM micrograph of a nanorods-arrays forming 30º with the normal to the substrate. These NRs were obtained by placing the substrate at 45º and a distance of 7 cm with respect to the precursor dispenser (cf. Figure 1).

The crystal structure of the NRs was analyzed by GA-XRD at an incident angle of 1º. **Figure 5** b) shows the XRD pattern corresponding to the material prepared at 407 K, where no peaks from crystalline titanium oxide or silver can be detected. Since for many applications of 1D TiO_2 nanostructures it is preferable to use the anatase phase of this

material, we subjected the obtained Ag@TiO$_2$ amorphous samples to a post annealing treatment at 673 K. Secondary and backscattered SEM images in **Figure 5** a) reveal that after this treatment part of the silver segregates as small nanoparticles on top of the NRs. Except for this modification of the metal distribution, the nanostructure morphology remained unaltered even if GAXRD (Figure 5 b) revealed the crystallization of both TiO$_2$ and silver.

Growth mechanism for supported Ag@TiO$_2$ NRs

Plasma deposition has been widely used for the controlled synthesis of carbon nanorods and nanotubes.[19-23] When used for this purpose, carbon species from a hydrocarbon plasma bind under the action of metal catalyst particles ending up with the formation of the 1D nanostructures.[37,38] Our original results concerning the formation of Ag@TiO$_2$ NFs on bulk silver substrates[26-28] were accounted for by a "volcano" mechanism with no intervention of catalytic effects and where the high mobility of the silver oxide formed during the silver pretreatment with an oxygen plasma was the key process. Although the formation of NRs grown on processable substrates reported here is in part congruent with this model, two additional specific features should be taken into account: i) the possibility to form vertical and tilted nanostructures and ii) the formation of quite homogeneous NRs arrays despite the inhomogeneity of the pre-oxidized silver substrates. **Figure 6** depicts a scheme to account for the formation of Ag@TiO$_2$ NRs on processable substrates. Two situations are considered depending on whether the substrate is normal to the incoming flux of material or it forms an angle with respect to this direction. These two situations will be discussed separately.

After plasma oxidation and heating, the silver seed layer (**Figure 6** Left) (steps t0 and t1) forms irregular and randomly distributed structures of silver and silver oxide nuclei. Since the amount of nucleation points is limited and its distribution random, the distribution of NRs obtained by PECVD of TiO$_2$ was rather homogeneous at a mesoscopic scale (step t2). According to the "volcano" mechanism the NRs growth takes place preferentially on top of silver oxide moieties which become reduced to metallic silver by reaction with the TTIP at

407 K. At this temperature, silver becomes mobile and flows within the growing NRs forming a channel in their interior (t3). Under these conditions, shadowing effects do not induce any change in the perpendicular orientation of the NRs but just in the preferential growth of some NRs with respect to others and producing an slight increment of the thickness at the tips of the nanorods (as observed in depositions for a long time Figure 4 d). Meanwhile the electrical field lines of the plasma sheath, coinciding with the preferential flow of precursor fragments favor the vertical growth of NRs. In comparison with the results obtained on bulk silver, the NRs fabricated on processable substrates have an inhomogenous inner core formed by the agglomeration of small nuclei and atoms of silver. We believe that the limited amount of silver available in the deposited seed layers hampers a continuous diffusion of the metal into the NRs and therefore the formation of a single crystalline core as reported for the $Ag@TiO_2$ NFs formed on a bulk silver substrate.

Figure 6 Right) shows a similar scheme describing the growth of tilted NRs. The major difference with the case of vertically aligned NRs is the angle that forms the substrate and the flux of incoming plasma species and precursor molecules and moieties. It must be bear in mind that at the working pressure, the mean free path of gas particles in the order of centimeters is in the same range that the distance between the dispenser and the substrates and that, therefore, collisions would not be very effective in randomizing the average incoming angle of particles. Thus, while plasma ions accelerated by the plasma sheath potential would tend to arrive perpendicular to the surface irrespective of the substrate orientation, on average, neutral gas and precursor species will arrive to the surface along a tilted trajectory with respect to the substrate[30] (Figure 6 t'1). Similarly to the deposition of columnar layers by physical vapor deposition at glancing angles (GLAD),[39] a tilted geometry is then obtained for the NRs (Figure 6 t'2 and t'3). We must note that in plasma activated growth the situation is more complex than in a conventional GLAD experiment because the incoming species are much less focused and the development of a plasma sheath at the surface tends to

counterbalance the tilted orientations. With regard to our previous formulation of the volcano mechanism of formation of NFs,[27] where plasma sheath effects were assumed as predominant, the present results support that shadowing effects associated with the preferential arrival the neutral particles can induce the tilting of the nanostructures and therefore may provide an additional means of controlling their orientation.

Wetting behavior of Ag@TiO$_2$ NR surfaces

A widely used approach for the fabrication of superhydrophobic coatings with a low adhesion to liquids is to increase their surfaces roughness and/or to create air-pockets within nanostructured surface features. Supported nanofibers and nanorods are ideal for this purpose because of their high inherent roughness and porosity.[40-42]

After aging by storage in dark, all the fabricated Ag@TiO$_2$ NR-arrays presented a superhydrophobic character (WCAs higher than 150º). **Figure 7** a) shows an example with a WCA close to 170º corresponding to NRs with a length of 900 nm, a width of 100 nm and a surface density of 100 nanorods per µm^2. A general tendency with these nanostructures was that the thicker the NRs forming the surfaces the smaller the WCA. This is illustrated in Figure 7 b) showing a micrograph of an array of 210 nm-thick and 835 nm-long NRs where the static WCA was 156º (advancing and receding angles of 159º and 150º, respectively). Since the WCA on flat TiO$_2$ thin films grown on flat silicon wafers by using the same PECVD procedure was ∼ 82º, it is possible to relate the superhydrophobicity of the nanorod surfaces with their dimensions and surface density.[40,42] For this analysis we have applied the classic models of Wenzel using the roughness as the main linking parameter between the real and the ideal WCAs of the surface (Equation 1) and Cassie-Baxter, this latter to take into account the effect of air trapped in the porous structure of the NRs film (Equation 2).[43,44] These models can be formulated as follows:

$$\cos\Theta' = r \cos\Theta \tag{1}$$

$$\cos\Theta' = -1 + \phi_S (1 + \cos\Theta) \tag{2}$$

where Θ' is the actual contact angle (e.g., 156º), Θ (i.e., 82º) the contact angle of an equivalent flat and compact surface (in our case the sample fabricated during the same experiment on a Si(100) wafer), r the roughness factor and ϕ_S the fraction of solid in contact with the liquid (see the scheme inserted in Figure 7 a). To calculate the roughness factor of our system we have modeled the individual nanowires as a vertical cylinder of mean height h = 835 nm and mean radius of r_0 = 105 nm. Thus, the area of a single Ag@TiO$_2$ NR-array is ca. A_{NR} = 5.51 x 10^5 nm^2. The roughness factor r is given by the ratio between the actual and geometrical area of the surface. When applied to a 1 µm x 1 µm surface, the total area (A_{total}) can be approximated by the relation established in Equation 3.

$$A_{total} = 1 \text{ x } 10^6 \text{ nm}^2 + N \cdot A_{NR} - N \cdot \pi r_0^2 \tag{3}$$

Where N corresponds to the number of NRs per µm^2. For the surface shown at Figure 3 d) N is about 60 NR µm^{-2} and therefore r = $A_{total}/A_{geometric}$ = 32. Taking this value of the roughness factor, through Equation 1 we get an equivalent contact angle $\Theta \sim 91$º, quite different from the actual WCA $\Theta' \sim 156$º. This difference and the slight hydrophilicity of the reference sample (i.e. Θ=82º, lower than the value of 90º usually taken as the transition between hydrophobicity and hydrophilicity) suggests that the superhydrophobic behavior of the original NR surfaces should be related with the air pockets trapped in the system.[44] This is equivalent to say that the superhydrophobic behavior of the Ag@TiO$_2$ NRs must be attributed to a Cassie-Baxter rather than to a Wenzel state. Since the factor ϕ_S in Equation 2, giving account of the solid fraction of the surface actually in contact with the drop, cannot be determined independently, the application of the Cassie-Baxter model to our surfaces requires to play with additional geometrical parameters. According to the scheme in Figure 7a) we assume that, in general water of droplets only penetrates the inter-NR space up to a certain depth and therefore does not reach the substrate surface.[31] According to this scheme, ϕ_S relates through h_w (length of

the inter NR space actually filled with water) with the area of the NRs in contact with water (A_{NR-W}) as presented in Equation 4.

$$\phi_S = A_{NR-W} / A_{total} = (N \cdot 2\pi r_0 \cdot h_w) / (\textit{Result Equation 3}) \qquad (4)$$

And therefore,

$$h_w = (A_{total} \cdot \phi_S) / (N \cdot 2\pi r_0) \qquad (5)$$

To estimate h_w from experimental measurements, ϕ_S is first calculated by substituing in Equation 2 the measured Θ and Θ' angles. For the example reported in Figure 7, this yields a value of $h_w \sim 60$ nm, meaning that in the original samples consisting of NRs with an average length of 835 nm, only a small fraction of this length is infiltrated with water.

Light induced wetting of Ag@TiO$_2$ surfaces

Since the pioneering work of Wang et al.[45] on the light induced transformation of the wetting angle of UV-irradiated TiO$_2$, much work has been devoted to both explaining the changes from hydrophobic to superhydrophilic upon light irradiation and to enhance the magnitude of this WCA variation by using nanostructured surfaces. The superhydrophobic character of the Ag@TiO$_2$ NRs surfaces represents an ideal situation to develop smart and processable surfaces with a wide and reversible change in WCA attainable by light irradiation.

To check the characteristics of this light induced transformation, we have followed the evolution of the WCA as a function of the irradiation time for samples where we have controlled the crystalline character of the TiO$_2$ shell. Figure 7b) shows the evolution of the WCA of Ag@TiO$_2$ amorphous and anatase NRs surfaces subjected to UV light irradiation for increasing periods of time. Results for an amorphous TiO$_2$ thin film have been included for comparison. It appears that in the three cases superhydrophilicity (WCA < 10º) is reached by illumination, although the kinetics of the process was different depending on the sample. The superhydrophilic transformation was much faster on the anatase sample, where WCAs lower than 10º where attained for 2 minutes of UV irradiation. This time dependence is in a good

agreement with previous studies with Ag@TiO$_2$ NFs surfaces grown on a silver substrates.[41] The transition from hydrophobic to hydrophilic was much slower on the amorphous Ag@TiO$_2$ NRs, in agreement with the lower photoactivity of amorphous TiO$_2$.[25b] In addition, the transformation process depicted two different kinetic regimes with a sharp inflexion point after irradiating for 200 min. We attribute the appearance of this sharp transition to the complete filling of the intercolumnar space after irradiation for this period of time. The following reasoning supports this hypothesis. According to Wang and many other researchers afterwards,[8, 45-47] the UV irradiation of a TiO$_2$ surface transforms it into superhydrophilic (i.e., WCA close to zero), independently on surface roughness and morphology. This transformation should also be expected for the Ag@TiO$_2$ NRs surfaces. According to Equs. (2, 4-5), taken Θ as the experimental (or extrapolated) angle determined for the irradiated TiO$_2$ thin film surface and Θ' the equivalent angle determined for the Ag@TiO$_2$ nanostructured surface, it is possible to calculate the h_w values for each irradiation time. The results of this calculation reported in Figure 7c) show that h_w progressively increases with irradiation time. When h_w reaches a value of approximately 800 nm, water must have penetrated completely the inter-NR space, so that the drop would not see any pocket of air. Under these conditions, the surface state cannot be described anymore by the Cassie-Baxter model and the wetting behavior changes abruptly. Experimentally, this situation is revealed by a sharp change in the WCA that drops from approximately 90º to 10º after 200 min of UV irradiation. As in previous examples,[9,29] the superhydrophobic-superhydrophilic conversion is fully reversible after storage of the samples in dark and dry conditions during few days.

Conclusion

The present work describes the growth at mild temperatures of Ag@TiO$_2$-NRs by plasma deposition of TiO$_2$ on conventional silicon or fused silica substrates, i.e. processable substrates, covered with silver. The NRs consist of an inner silver core and an outer TiO$_2$

layer. It is proved that the chemical state and thickness of the silver layer and other experimental variables such as the amount of precursor and the deposition time can be varied to tune the morphology of the NRs.

The reported methodology of NR formation implies a three-step plasma process starting with the deposition of a silver layer on top of the substrate, its plasma oxidation and the deposition of TiO_2 by PECVD. An outstanding feature of the process is that both vertical and tilted $Ag@TiO_2$ nanorods can be produced in high density with a quite homogeneous length and thickness distribution. The growth mechanism proposed to account for this phenomenology agrees in part with the steps of a volcano-type mechanism already used to account for the formation of $Ag@TiO_2$-NFs and $Ag@ZnO$-NRs, incorporating as an additional effect the existence of shadowing effects generated by the arrival onto the surface of a preferentially oriented flux of precursor molecules and neutral species of the plasma. The superhydrophobic behavior depicted by the $Ag@TiO_2$-NRs surfaces has been described by assuming a Cassie-Baxter state. This has permitted to estimate the degree of penetration of water within the inter-nanorod space. Using a similar reasoning, we have explained the change in WCA observed when the surfaces are UV irradiated as resulting from an increase in the penetration length of water within the NRs structure and, at the end, from its complete filling when the surface state cannot be described anymore by a Cassie-Baxter model.

[1] a) X. Chen, *Chin. J. Catal.* **2009**, *30*, 839; b) C. Cao, C. Hu, X. Wang, S. Wang, Y. Tian,

H. Zhang, *Sens. Act. B* **2011**, *156*, 114; c) K. S. Brammer, S. Oh , J. O. Gallagher, S. Jin,

Nano Lett. **2008**, *8*, 786.

[2] J. L. Campbell, M. Breedon, K. Latham, K. Kalantar-Zadeh,

Langmuir **2008**, *24*, 5091.

[3] B. Kakade, R. Mehta, A. Durge, S. Kulkarni and V. Pillai, *Nano*

Lett. **2008**, *8*, 2693.

[4] N. Verplanck, E. Galopin, J. C. Camart, V. Thomy, Y. Coffinier, R. Boukherroub, Nano

Lett. **2007**, *7*, 813.

[5] T. N. Krupenkin, J. A. Taylor, T. M. Schneider, S. Yang, Langmuir **2004**, *20*, 3824.

[6] H. Z. Wang, Z. P. Huang, Q. J. Cai, K. Kulkarni, C.-L. Chen, D. Carnahan, Z. F. Ren,

Carbon **2010**, *48*, 868.

[7] J. Yang, Z. Zhang, X. Men, X. Xu, X. Zhu, *Carbon* **2011**, *49*, 19.

[8] X. Feng, J. Zhai, L. Jiang, *Angew. Chem. Int. Ed.* **2005**, *44*, 5115.

[9] A. Borras, A. Barranco, A. R. Gonzalez-Elipe, *Langmuir* **2008**, *24*, 8021.

[10] S. Yoo, S. A. Akbar, K. H. Sandhage, *Adv. Mater.* **2004**, *16*, 260.

[11] J. Joo, S. G. Kwon, T. Yu, *J. Phys. Chem. B* **2005**, *109*, 15297.

[12] C. Dames, B. Poudel, W. Z. Wang, J. Y. Huang, Z. F. Ren, Y. Sun, J. I. Oh, C. Opeil, M.

J. Naughton, G. Chen, *Appl. Phys. Lett.* **2005**, *87*, 031901.

[13] P. Hoyer, *Langmuir* **1996**, *12*, 1411.

[14] D. Gong, C. A. Grimes, O. K. Varghese, W. Hu, R. S. Singh, Z. Chen, E. C. Dickey, *J. Mater. Res.* **2001**, *16*, 3331.

[15] G. H. Du, Q. Chen, R. C. Che, Z. Y. Yuan, L. M. Peng, *Appl. Phys. Lett.* **2001**, *79*, 3702.

[16] T. Kasuga, M. Hiramatsu, A. Hoson, T. Sekino, K. Niihara, *Adv. Mater.* **1999**, *11*, 1307.

[17] J. Du, J. Zhang, Zh. Liu, B. Han, T. Jiang, Y. Huang, *Langmuir* **2006**, *22*, 1307.

[18] J. Zhou, Y. Ding, S. Z. Deng, L. Gong, N. S. Xu, Z. L. Wang, *Adv. Mater.* **2005**, *17*, 2107.

[19] K. Ostrikov, U. Cvelbar, A. B. Murphy, *J. Phys. D: Appl. Phys.* **2011**, *44*, 174001.

[20] K. Ostrikov , E. C. Neyts, M. Meyyappan, *Advances in Physics* **2013**, *62*, 113.

[21] G. Zhong, M. Tachiki, H. Umezawa, T. Fujisaki, H. Kawarada, *Chem. Vap. Deposition* **2004**, *10*, 125.

[22] K. B. K. Teo, S.-B. Lee, M. Chhowalla, V. Semet, V. T. Binh, O. Groening, M. Castignolles, A. Loiseau, G. Pirio, P. Legagneux, D. Pribat, D. G. Hasko, H. Ahmed, G. A. J. Amaratunga, W. I. Milne*, Nanotechnol.* **2003**, *14*, 204.

[23] H. S. Uh, S. S. Park, *Thin Solid Films* **2006**, *504*, 50.

[24] a) A. Borras, J. R. Sanchez-Valencia, J. Garrido-Moliner, A. Barranco, A. R. Gonzalez-Elipe, *Micro. Meso. Mater.* **2009**, *118*, 314; b) A. Borras, R. Alvarez, J. R. Sanchez-Valencia, J. Ferrer, A. R. Gonzalez-Elipe, *Micro. Meso. Mater.* **2012**, *160*, 1.

[25] a) A. Borras, J. R. Sanchez-Valencia, R. Widmer, V. J. Rico, A. Justo, A. R. Gonzalez-Elipe, *Crys. Growth Design* **2009**, *9*, 2868-2876; b) A. Borras. A. R. Gonzalez-Elipe, *Langmuir* **2010**, *26*, 15875

[26] A. Borras, A. Barranco, F. Yubero, A. R. Gonzalez-Elipe, *Nanotechnol.* **2006**, *17*, 3518.

[27] A. Borras, A. Barranco, J. P. Espinos, J. Cotrino, J. P. Holgado, A. R. Gonzalez-Elipe, *Plasma Process. Polym.* **2007**, *4*, 515.

[28] A. Borras, M. Macias-Montero, P. Romero-Gomez, A. R. Gonzalez-Elipe, *J. Phys. D.* **2011**, *44*, 174016.

[29] M. Macias-Montero, A. Borras, Z. Saghi, P. Romero-Gomez, J. R. Sanchez-Valencia, J. C. Gonzalez, A. Barranco, P. Midgley, J. Cotrino, A. R. Gonzalez-Elipe, *J. Mater. Chem.* **2012**, *22*, 1341.

[30] M. Macias-Montero, A. Borras, Z. Saghi, J. P. Espinos, A. Barranco, J. Cotrino, A. R. Gonzalez-Elipe, *Nanotechnol.* **2012**, *23*, 255303.

[31] M. Macias-Montero, A. Borras, R. Alvarez, A. R. Gonzalez-Elipe, *Langmuir* **2012**, *28*, 15047.

[32] A. Barranco, J. Cotrino, F. Yubero, J. P. Espinos, J. Benitez, C. Clerc, A. R. Gonzalez-Elipe, *Thin Solid Films* **2001**, *401*, 150.

[33] M. Alcaire, J. R. Sanchez-Valencia, F. J. Aparicio, Z. Saghi, J. C. Gonzalez-Gonzalez, A. Barranco, Y. Oulad-Zian, A. R. Gonzalez-Elipe, P. Midgley, J. P. Espinos, P. Groening, A. Borras, *Nanoscale* **2011**, *3*, 4554.

[34] F. Gracia , J. P. Holgado, A. Caballero, A. R. Gonzalez-Elipe, *J. Phys. Chem. B*, **2004**, *108*, 17466.

[35] M. Macias-Montero, A. N. Filippin, Z. Saghi, F. J. Aparicio, A. Barranco, J. P. Espinos, F. Frutos, A. R. Gonzalez-Elipe, A. Borras, *Adv. Funct. Mater.* **2013**, DOI: 10.1002/adfm.201301120.

[36] K. Moore, C. B. Clemons, K. L. Kreider, G. W. Young, *J. Appl. Phys.* **2007**, *101*, 064305.

[37] G. Zhong, M. Tachiki, H. Umezawa, T. Fujisaki, H. Kawarada, *Chem. Vapor Depos.* **2004**, *10*, 125.

[38] K. B. K. Teo, S. B. Lee, M. Chhowalla, V. Semet, V. T. Binh, O. Groening, M. Castignolles, A. Loiseau, G. Pirio, P. Legagneux, D. Pribat, D. G. Hasko, H. Ahmed, G. A. J. Amaratunga, W. I. Milne, *Nanotechnol.* **2003**, *14*, 204.

[39] L. Gonzalez-Garcia, J. Parra-Barranco, J. R. Sanchez-Valencia, A. Barranco, A. Borras, A. R. Gonzalez-Elipe, M. C. Garcia-Gutierrez, J. J. Hernandez, D. R. Rueda, T. A. Ezquerra, *Nanotechnology* **2012**, *23*, 255701.

[40] A. Lafuma, D. Quere, *Nat. Mater.* **2003**, *2*, 457.

[41] A. Borras, A. Barranco and A. R. Gonzalez-Elipe, *Langmuir* **2008**, *24*, 8021.

[42] A. Borras, P. Groening, J. R. Sanchez-Valencia, A. Barranco, J. P. Espinos, A. R. Gonzalez-Elipe, *Langmuir* **2010**, *26*, 1487.

[43] Y. Tak, K. Yong, C. Park, *J. Electrochem. Soc.* **2005**, *152*, G794.

[44] M. Haupt, A. Ladenburger, R. Sauer, K. Thonke, R. Glass, W. Roos, J. P. Spatz, H. Rauscher, S. Riethmuller, M. Moller, *J. Appl. Phys.* **2003**, *93*, 6252.

[45] R. Wang, K. Hashimoto, A. Fujishima, M. Chikuni, E. Kojima, A. Kitamura, M. Shimohigoshi, T. Watanabe, *Nature* **1997**, *388*, 431.

[46] N. Stevens, C. I. Priest, R. Sedev, J. Ralston, *Langmuir* **2003**, *19*, 3272.

[47] D. Wang, Y. Liu, X. Liu, F. Zhou, W. Liu, Q. Xue, *Chem. Commun,.* **2009**, 7018.
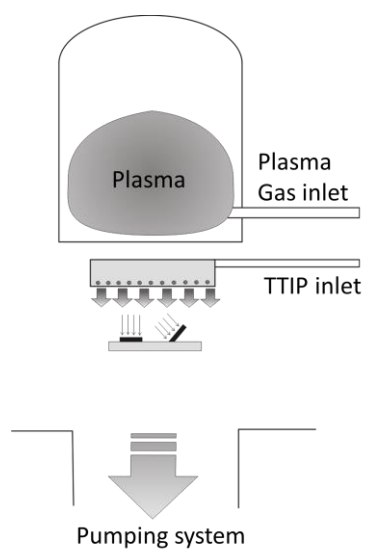
Figure 1. Scheme of the experimental setup showing two different orientations of the sample substrates with respect to the precursor flow imposed by the pumping system.
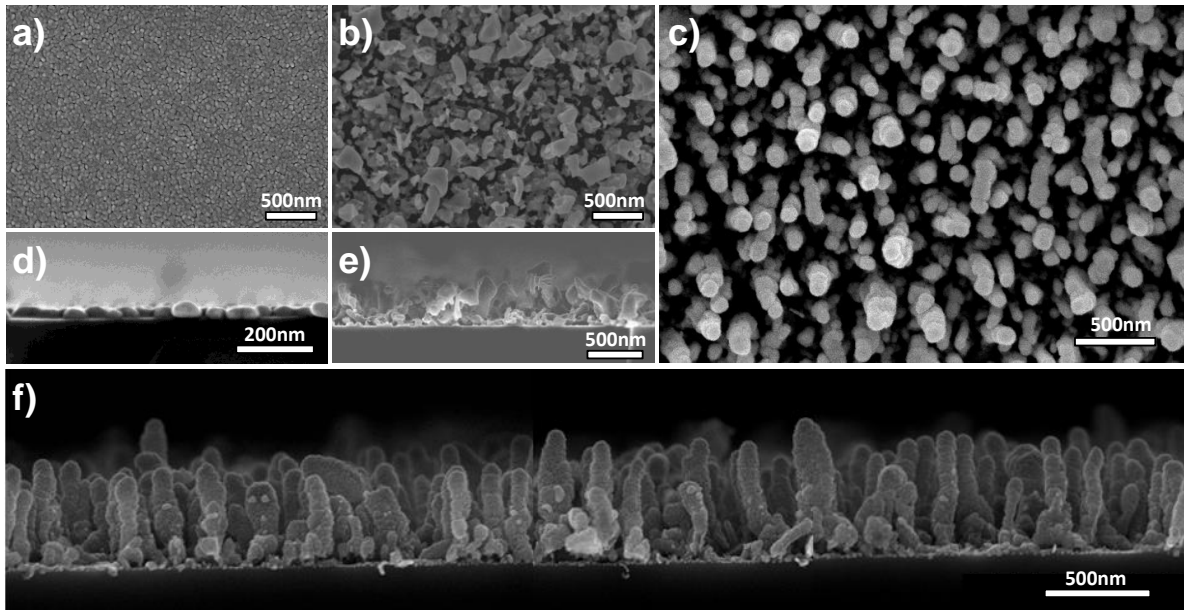
Figure 2. Cross sections and normal view SEM micrographs of sputtered silver as prepared (a and d); sputtered silver after 30 minutes of oxygen plasma treatment at 407 K (b and e); Ag@TiO$_2$ NRs formed by deposition at 407 K (c and f).
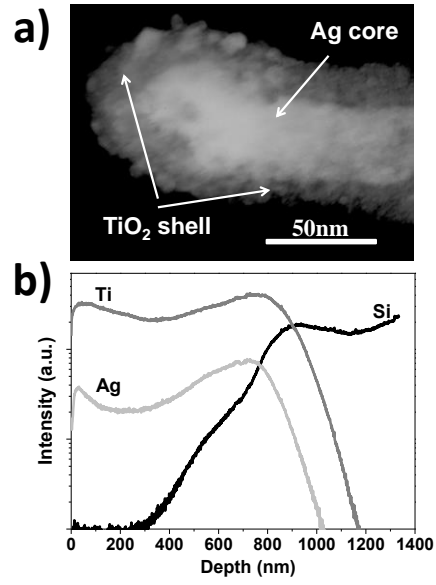
Figure 3. a) TEM micrograph of an isolated NR showing a silver core and a TiO$_2$ shell; b) ToF-SIMS analysis of a characteristic vertical aligned Ag@TiO$_2$ sample.
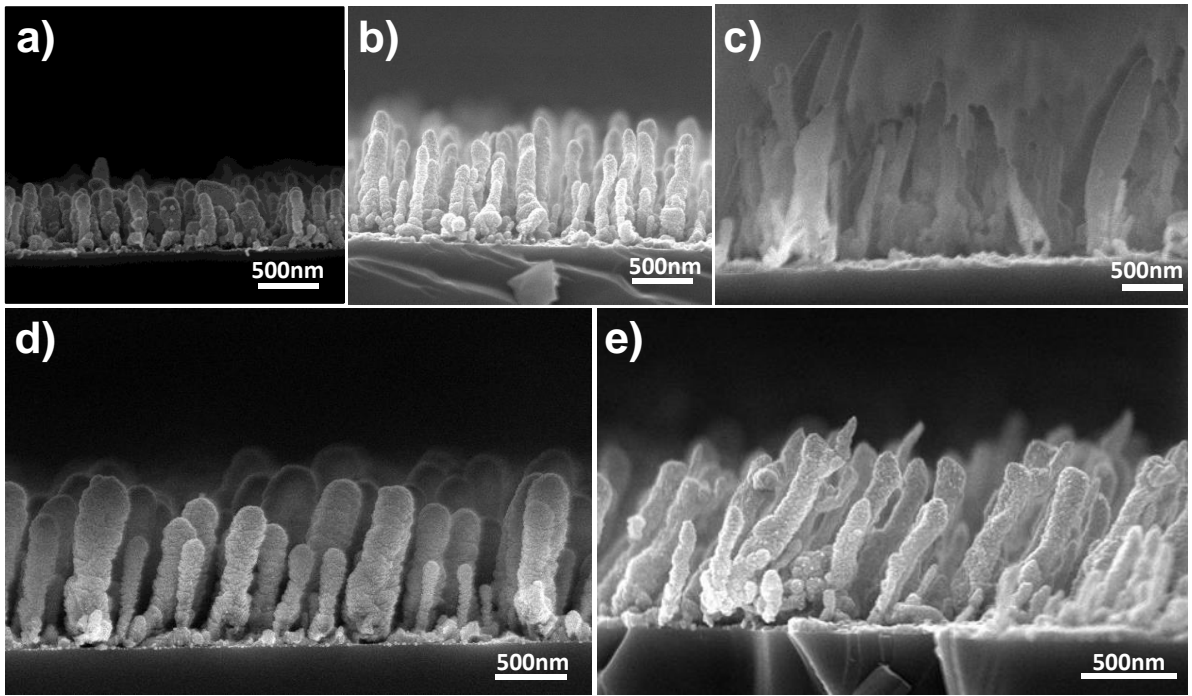
Figure 4. a), b) and c) SEM micrographs of the NRs grown with different doses of precursor controlled by chaning the oxygen flow bubbled through it: 0.5, 1 and 2.5 sccm respectively; d) NRs formed after a long plasma deposition time (120 minutes); e) Tilted structures formed by changing the orientation of the substrates with respect of the precursor flow according to the scheme in Figure 1.
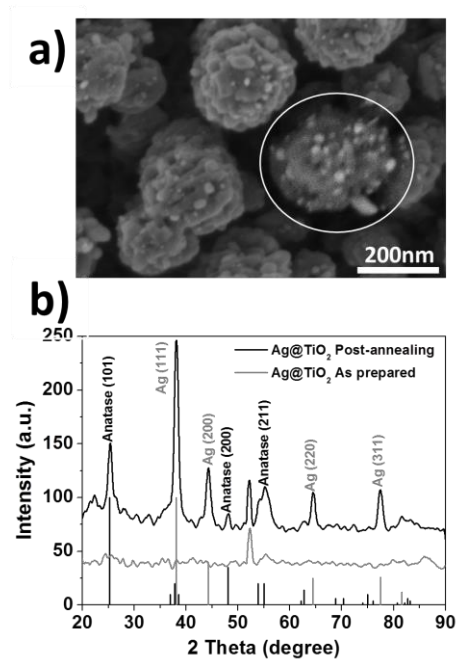
Figure 5. a) Secondary electron SEM image of annealed Ag@TiO$_2$ NRs with backscattered electrons image as an inset, b) XRD spectra of the as-grown and annealed NRs. The peaks of anatase and silver are conveniently assigned in the diagrams.
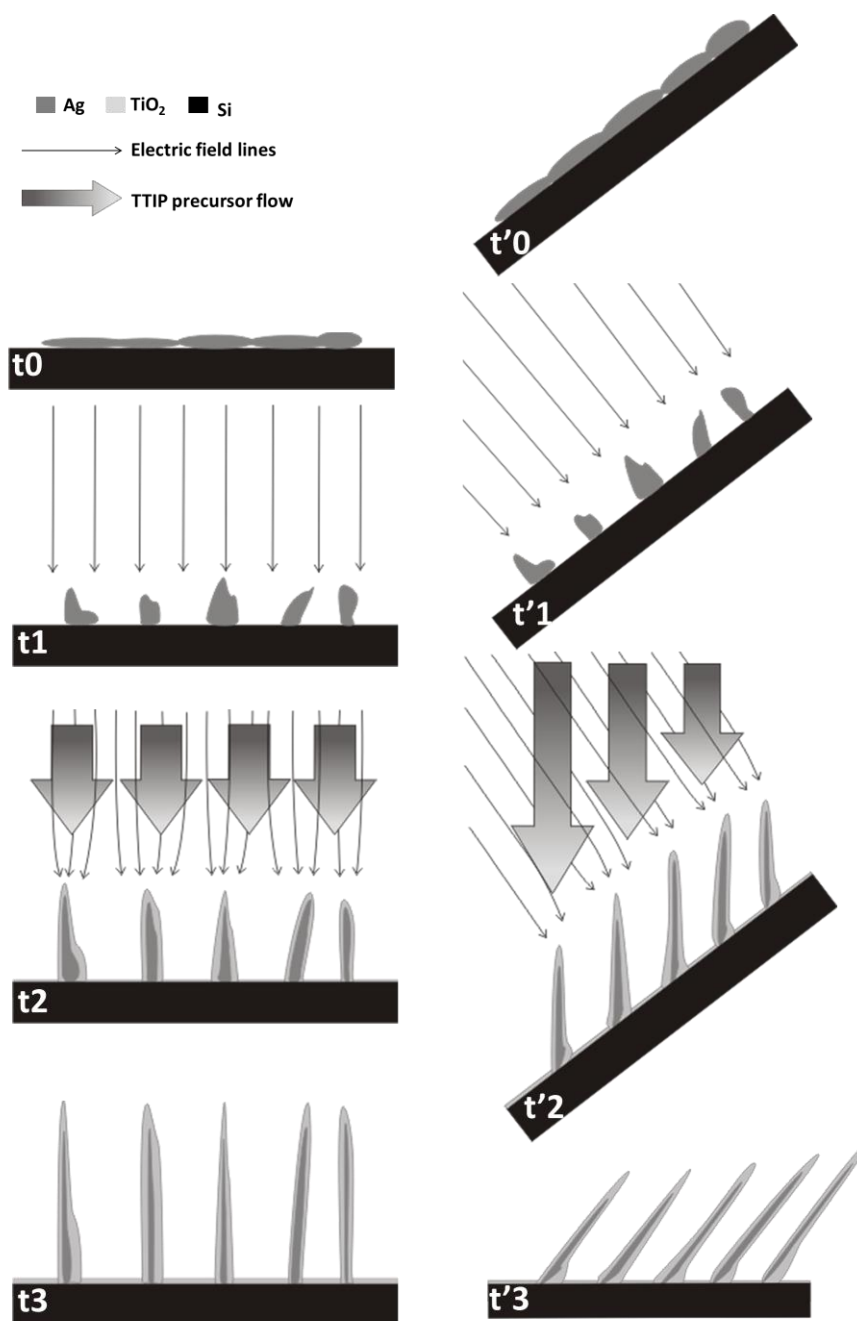
Figure 6. Different stages of the Ag@TiO$_2$ NRs formation based on the volcano-type mechanism for vertical (left) and tilted (right) growth. Thick arrows describe the preferential direction of the precursor flow towards the substrate. Thin arrows represent the electrical filed lines associated to the plasma sheath.
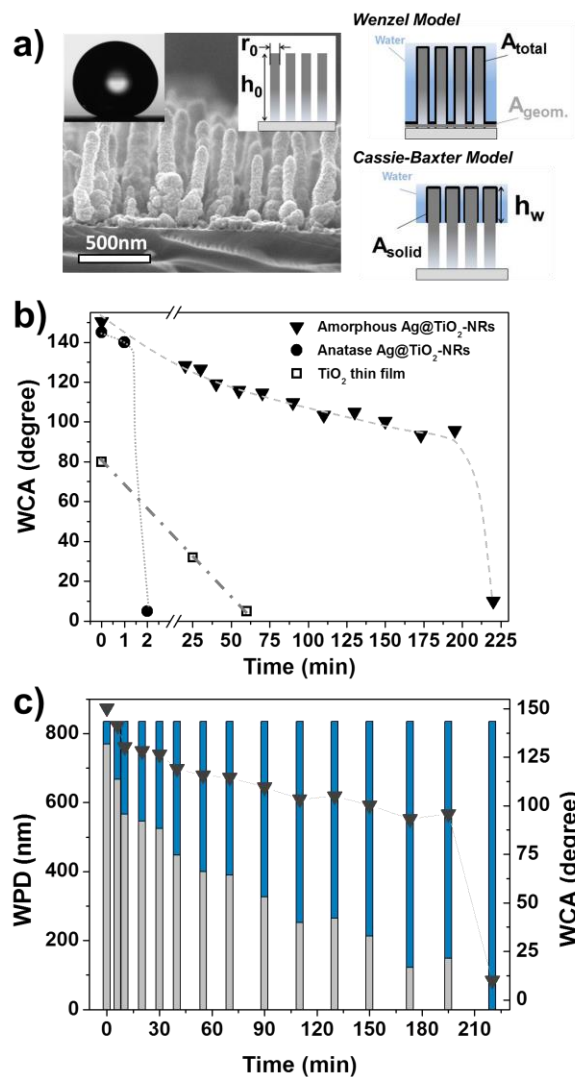
Figure 7. a) Water droplet formed on top of a Ag@TiO$_2$ NRs sample with a contact angle of 170° and SEM micrograph of the array layer. The scheme shows the definition of formula parameters by the application of the Wenzel and Cassie-Baxter models. b) Water contact angel evolution under ultraviolet light irradiation for Ag@TiO$_2$ amorphous and anatase NRs as and a flat amorphous TiO$_2$ thin film taken as a reference. c) Water penetration depth (WPD) evolution under ultraviolet light irradiation and WCA evolution (triangle symbols). The bars illustrate the degree of penetration of water within the inter-NR space.

The growth of vertical and tilted Ag@TiO$_2$ core@shell nanorods by PECVD is demonstrated. Control on the experimental parameters allows the formation of NRs with tailored morphology on processable substrates at mild temperature. High density NRs surfaces present superhydrophobic behavior tunable till superhydrophilic under UV light. Wetting mechanism and superhydrophobic-hydrophilic transition are explained within the Cassie-Baxter and Wenzel models.

Manuel Macias-Montero, Ana Borras,[*] Pablo Romero-Gomez, Jose Cotrino, Fabian Frutos and Agustin R. Gonzalez-Elipe

Plasma deposition of superhydrophobic Ag@TiO$_2$ core@shell nanorods on processable substrates
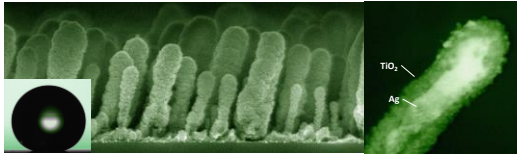
Supporting Information

for *Abbrev. J. Title*, DOI: 10.1002/((please add journal code and manuscript number))

Title ((no stars))

Author(s), Corresponding Author(s)* ((write out first and last name))

((Please insert your Supporting Information text/figures here. Please note: Supporting Display items, should be referred to as Figure S1, Equation S2, etc., in the main text…)